Photocatalytic Property and Electronic Structure of Triple-Layered Perovskite Tantalates, $MCa_2Ta_3O_{10}$ (M = Cs, Na, H, and $C_6H_{13}NH_3$)

Masato Machida,* Tomohiro Mitsuyama, and Keita Ikeue

Department of Applied Chemistry and Biochemistry, Faculty of Engineering, Kumamoto University, Kumamoto 860-8555, Japan

Shigenori Matsushima

Kitakyushu National College of Technology, Kitakyushu 802-0985, Japan

Masao Arai

National Institute for Research in Inorganic Materials, Tsukuba 305-0044, Japan

Received: November 10, 2004; In Final Form: February 2, 2005

The Dion−Jacobson series of triple-layered perovskite tantalates ($MCa_2Ta_3O_{10}$, M = Cs, Na, H, and $C_6H_{13}NH_3$) were synthesized to evaluate their photocatalytic activity for overall water splitting to evolve H_2/O_2 under UV irradiation. The photocatalytic activity was susceptible to the hydration of interlayer space. The hydrous Na phase exhibited much higher activity (H_2: 308 μmol·h^{-1}) compared to the anhydrous Cs phase (24 μmol·h^{-1}) and the hydrous H phase (22 μmol·h^{-1}) in the presence of 0.5 wt % Ni impregnated. H_2O/D_2O isotopic experiment suggested that the hydrated interlayer plays as an active site for water splitting, where the high mobility of water molecule in the interlayer should correlate with the total photocatalytic activity. The FLAPW electronic structure calculation demonstrated that the terminating oxygen site, O(4), which faces to the interlayer space, contributes largely to the top of the valence band. Judging from comparison with the double-layered tantalates, $MLaTa_2O_7$, in our previous study, the contribution of terminating oxygen site to the band structure is supposed to depend on the number of perovskite layers.

Introduction

Ion-exchangeable layered perovskites are composed of alternative stacking of a two-dimensional perovskite slab with different numbers of layers and monovalent cations. There are two different typical structures, the Dion−Jacobson series ($A'[A_{n-1}B_nO_{3n+1}]$) and the Ruddlesden−Popper series ($A'_2[A_{n-2}B_nO_{3n+1}]$).[1−5] A wide variety of compounds in these structural families include titanates, niobates, and tantalates with the d^0 electronic configuration, which can be used as photocatalysts.[6−15] In the applications of such layered ion-exchangers to photocatalytic water splitting, the role of interlayer is of general interest because of the hydrated structure. It is already reported that several layered perovskites, such as $K_4Nb_6O_{17}$[10] or $K_2La_2Ti_3O_{10}$,[11] are highly active for overall water splitting, because their interlayer space is easily hydrated to produce active sites responsible for photocatalytic water splitting. However, a different situation was observed for hydrated $NaLaTa_2O_7$, the activity of which is less than that of the anhydrous $RbLaTa_2O_7$.[15] Thus, the effect of interlayer hydration is not always the predominant factor. The combination of experimental and theoretical approaches is strongly requested to gain an understanding of the chemistry of interlayer in photocatalytic processes from material viewpoints.

The purpose of our study is to elucidate the relationship between photocatalytic property and hydrated layered structure. In this regard, Dion−Jacobson-type tantalates are very useful because a series of the same structural unit with hydrous and anhydrous interlayer is available. The present work has been directed to study the effect of ion exchange of interlayer cations (M) on the photocatalytic property of triple-layered perovskite tantalates ($MCa_2Ta_3O_{10}$) in relation to their electronic and crystal structures. The materials with four different monovalent cations (M = Cs, Na, H, and $C_6H_{13}NH_3$) were synthesized to use them as photocatalysts for water splitting. The results were compared with those for double-layered tantalates ($MLaTa_2O_7$) in our previous study.[14,15]

Experimental Section

Sample Preparation and Characterization. The synthesis of $CsCa_2Ta_3O_{10}$ was conducted by a conventional solid-state procedure according to that reported by Toda et al.[16,17] Powder mixtures of carbonates (Cs_2CO_3, $CaCO_3$, 99%) and oxide (Ta_2O_5, 99.99%) were calcined at 1000 °C for 10 h in air. As-prepared Cs phase was ion-exchanged in molten $NaNO_3$ at 400 °C to convert into a Na phase, which was subsequently washed with distilled water. Since the resultant tantalate was a hydrated phase, which contains water in the interlayer, heat treatment at 500 °C was conducted in vacuo to obtain a dehydrated phase. A protonated compound (a H phase) was obtained by leaching the hydrated Na phase in 1 M HCl at room temperature for 1 week. The acid solution was refreshed every 2 days. The resultant solid was washed with distilled water and dried at 60 °C in air. The H phase thus obtained was then stirred in an aqueous solution of 5 M $C_6H_{13}NH_2$ at room temperature for a week to prepare a $C_6H_{13}NH_3$-exchanged phase.

* Corresponding author. Fax/tel: +81-96-342-3651; e-mail: machida@chem.kumamoto-u.ac.jp.

10.1021/jp044833d CCC: $30.25
Published on Web 03/25/2005

Thermogravimetric analysis (TG, Rigaku 8120) and X-ray analysis (EDX, Horiba MESA-500W) were conducted to determine water content and chemical composition, respectively. The crystal structure was identified by use of a powder XRD (Rigaku Multiflex) with monochromated CuK_α radiation (30 kV, 20 mA). Diffuse reflectance spectra were recorded with a Jasco V-550 UV−vis spectrometer. The optical band gap energy was calculated from the onset of absorption edge. The microstructure was observed by FE-SEM (Hitachi 4100). The BET surface area was determined by measuring N_2 adsorption isotherm at −196 °C.

The Ni-loaded catalyst was prepared by impregnation of as-prepared $MCa_2Ta_3O_{10}$ (M = Cs, Na, and H) with an aqueous solution of $Ni(NO_3)_2$ (reagent grade). The impregnated sample was then submitted to reduction in a stream of H_2 at 500 °C and subsequent reoxidation in a stream of O_2 at 200 °C to prepare partially oxidized nickel (NiO_x) catalysts.[18,19] The loading amount of Ni metal was from 0.1 to 2.0 wt %. Characterization of Ni species was done by XPS (VG Sigmaprobe spectrometer using Al Kα radiation, 15 kV, 7 mA) and TEM (JEOL 2000FX).

Electronic Structure Calculation. The first-principle approach in the present study is based on the FLAPW method within the local density approximation (LDA)[20] to the density function theory. The calculation of the electronic structure was conducted by the use of the WIEN2k package,[21] the results of which include a fully optimized ground-state structure obtained with total energy and atomic forces, band structure, and densities of states, as described in our previous papers.[22,23] The crystallographic parameters for the calculation, including lattice parameters and atomic positions, were those reported by Toda et al.[16,17] The parameters of individual atoms were optimized prior to the calculation using the MS Castep package (Accelrys).

Photocatalytic Reaction. The photocatalytic H_2 evolution from water was conducted in an inner irradiation quartz cell, which was connected to a closed gas-circulating system (dead volume: 250 cm^3) consisting of a circulation pump, a pressure sensor, gas sampling valves, and stainless steel tubing. A powder sample of the tantalate (0.2 g) was suspended in distilled water (200 cm^3) in the cell by use of a magnetic stirrer. Prior to the reaction, the mixture was deaerated by evacuation and then flushed with Ar gas (20 kPa) repeatedly to remove O_2 and CO_2 dissolving in water. The reaction was carried out by irradiating the mixture with light from a 400 W high-pressure Hg lamp. Gas evolution was observed only under photoirradiation, being analyzed by an online gas chromatograph (Shimadzu, TCD, Ar carrier, MS-5A and Porapak-Q columns). Any contamination from air was confirmed negligible during at least 50 h of photoreactions. The rate of photocatalytic gas evolution was determined for an initial 8-h period.

Results and Discussion

Crystal Phases of $MCa_2Ta_3O_{10}$. The XRD patterns and chemical compositions of $MCa_2Ta_3O_{10}$ (M = Cs, Na, H, and $C_6H_{13}NH_3$) are shown in Figure 1 and Table 1, respectively. As-calcined compounds, $CsCa_2Ta_3O_{10}$ (Figure 1a), consisted of a single phase of layered perovskite, the diffraction peaks of which were indexed on the basis of the tetragonal cell with the P4/*mmm* space group. The value of d_{001}, 1.51 nm, corresponds to the stacking periodicity of a triple-layer perovskite slab (see Figure 2). The Na phase, $NaCa_2Ta_3O_{10}$, was not obtained directly by the solid-state reaction of carbonate/oxide mixtures but was produced successfully by ion exchange of $CsCa_2Ta_3O_{10}$ in molten sodium nitrate at 400 °C (Table 1). As can be judged from Figure 1b, the Na phase shows a significant shift of diffraction peaks in accord with the transformation from P4/*mmm* to I4/*mmm*, which is consistent with the result reported by Toda et al.[16,17] This was accompanied by expansion of the interlayer distance from 1.51 to 1.72 nm, because 1.86 mol-$H_2O{\cdot}mol^{-1}$ was incorporated into the interlayer during washing in water. The formation of the hydrated Na phase is very similar to the double-layered compound, $MLaTa_2O_7$.[15] Furthermore, Na ions in the interlayer could be replaced by H (>98%) during repeated treatment in 1 M HCl. This resulted in a shift of the (00*l*) peaks to the higher 2θ because of the difference of ionic radius between Na^+ and H^+ (Figure 1c). The H phases possess the hydrous interlayer with 0.38 mol-$H_2O{\cdot}mol^{-1}$ (Table 1). The interlayer distance was then significantly expanded to 2.85 nm by following intercalation of $C_6H_{13}NH_3^+$ (ca. 0.6 $mol{\cdot}mol^{-1}$, Figure 1d). The corresponding interlayer spacing of ca. 1.7 nm is much larger than the chain length of *n*-hexylammonium ion (ca. 1.0 nm), suggesting the tilting bilayer configuration of alkyl chains in the interlayer.

The microstructure of exchanged tantalates (M = Cs, Na and H) was observed by SEM, which is included in the Supporting Information (Figure S1). Well-crystallized submicron particles

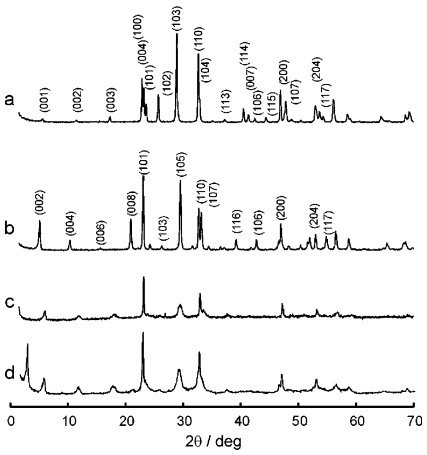

Figure 1. Powder XRD patterns of $MCa_2Ta_3O_{10}$ with (a) M = Cs, (b) Na, (c) H, and (d) $C_6H_{13}NH_3$.

TABLE 1: Chemical Composition of Layered Tantalates[a]

Cs phase	$Cs_{0.97}Ca_{2.00}Ta_3O_{10}$
Na phase	$Cs_{0.03}Na_{0.91}Ca_{1.97}Ta_3O_{10}{\cdot}1.86H_2O$
H phase	$Cs_{0.03}Na_{0.10}\,H_{0.87}Ca_{2.11}Ta_3O_{10}{\cdot}0.38H_2O$

[a] Oxygen nonstoichiometry is not considered.

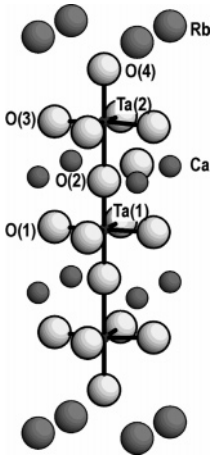

Figure 2. Crystal structure of $RbCa_2Ta_3O_{10}$ with layered perovskite structure.

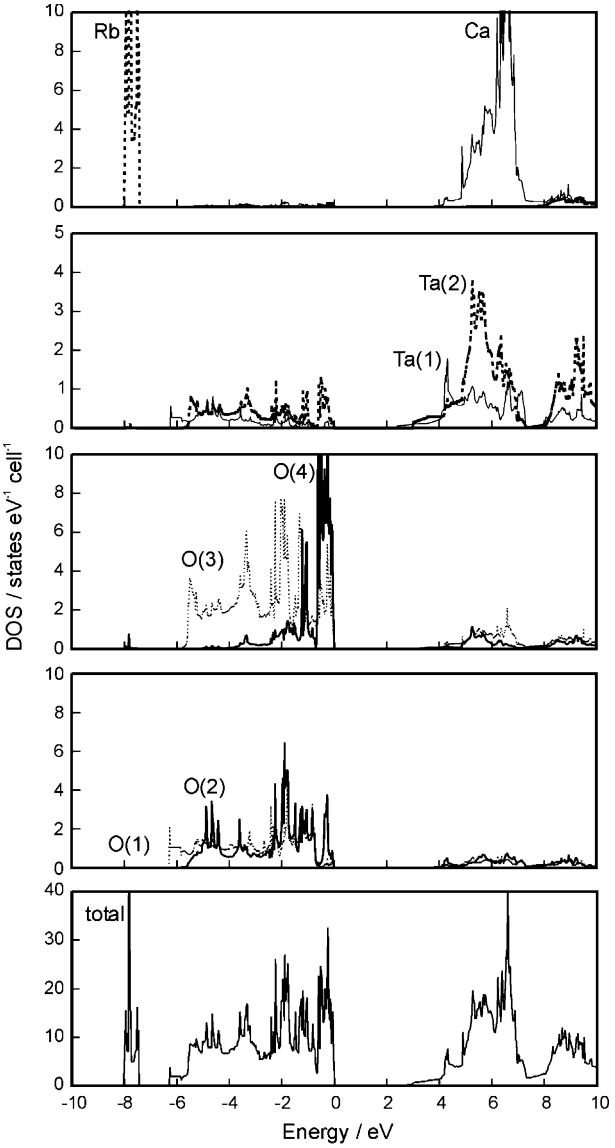

Figure 3. Total and partial density of states (DOS) for $RbCa_2Ta_3O_{10}$ calculated by FLAPW method.

with planar morphology showed no obvious change after ion exchange. Their BET surface areas were in the range of 2−4 $m^2 \cdot g^{-1}$. Thus, difference in photocatalytic activity arising from the crystal size and morphology can be neglected.

Calculated Electronic Structure. The electronic structure was studied by using a Rb-type isomorph of Dion−Jacobson series $RbCa_2Ta_3O_{10}$ (P4/*mmm*, $a = 0.387$ nm, $b = 1.504$ nm)[16,17] as shown in Figure 2. This is constructed by alternative stacking of a triple-corner-shared TaO_6 octahedra and a monatomic Rb layer along the *c* axis. Each Rb ion is coordinated by eight oxygens, O(4), of TaO_6 octahedra in adjacent two perovskite slabs. There are four different oxygen sites: O(2) bridging Ta(1) and Ta(2) with different distances (Ta(1)−O(2) 0.1835 nm, Ta(2)−O(2) 0.2430 nm), O(1) and O(3) forming an infinite two-dimensional TaO_2 network, and O(4) facing to the interlayer space. The different Ta−O distances cause a large distortion in the TaO_6 octahedra, which is characteristic of the layered structure.

On the basis of the crystal structure, the electronic structure of $RbCa_2Ta_3O_{10}$ was studied by the first-principle calculation using the FLAPW method. Figure 3 shows calculated partial and total density of states (DOS) of $RbCa_2Ta_3O_{10}$. The top of valence band (VB) is set at zero on the abscissa and is referred to as valence band edge. The states in the valence band region from ca. −6 to 0 eV are mainly composed of the O2p orbital, which is hybridized with Ta5d, whereas the contributions of Rb and Ca orbitals appear to be negligible. The partial DOS of four types of oxygen sites distribute very differently depending on their coordination environment and interatomic distances. The similar distributions of the O(1), O(3), and Ta partial DOS curves in this energy region suggest a considerable hybridization between O2p and Ta5d orbitals in a two-dimensional Ta−O network along the layer (//*ab*). This is contrast to the discrete Ta(2)−O(4) bond, which is partitioned by every interlayer. The O(2) DOS is less intense relative to others because of the greatest Ta(2)−O(2) distances (Table 2).

TABLE 2: Interatomic Distance of $RbCa_2Ta_3O_{10}$[a]

Ta(1)−O(1)	0.1929 nm
Ta(1)−O(2)	0.1835 nm
Ta(2)−O(2)	0.2430 nm
Ta(2)−O(3)	0.1951 nm
Ta(2)−O(4)	0.1813 nm

[a] References 16 and 17.

TABLE 3: Properties and Photocatalytic Activity of $MCa_2Ta_3O_{10}$

M		Cs^+	Na^+	H^+	$C_6H_{13}NH_3^+$
d[a]/nm		1.51	1.72	1.44	2.85
n[b]/mol·mol^{-1}		0	1.86	0.38	
E_g/eV		4.1	4.3	4.2	4.0
rate[c]	H_2	7.6	12.2	2.6	110.3
/μmol·h^{-1}	O_2	2.2	7.6	0.7	0
rate[d]	H_2	23.9	308.4	22.2	
/μmol·h^{-1}	O_2	10.3	157.7	5.2	

[a] Interlayer distance. [b] Interlayer H_2O. [c] Ni-unloaded. [d] 0.5 wt % Ni loaded. Rate was determined from H_2/O_2 evolution during initial 8-h photoirradiation.

The conduction band (CB) in the energy range above 3 eV mainly consists of Tad. The Ta partial DOS is largely ascribable to 5d orbitals, which are divided into two distribution peaks at 3−7 eV and 8−10 eV as a result of the crystal field splitting in the octahedral TaO_6 environment. The similar double-peak distributions in the four O partial DOS in this energy region support the large hybridization between O2p and Ta5d. Above the main weight of the Ta5d band, a strong and narrow peak due to the Ca orbital was observed, but the contribution to the band gap transition should be negligible.

Band Gap Energy and Photocatalytic Activity. Table 3 compares the optical band gap energy, E_g, photocatalytic activity for water splitting of $MCa_2Ta_3O_{10}$ (M = Cs, Na, H, and $C_6H_{13}NH_3$). The constant E_g about 4 eV irrespective of different M can be explained on the basis of the electronic structure, where the valence band and the conduction band consist primarily of O2p and Ta5d, respectively (Figure 3). Therefore, the E_g corresponds to the gap between Ta5d and O2p. On the other hand, the interlayer cation is negligibly associated with the values of E_g, because the Cs s and p orbitals form a high-lying antibonding band and a bonding band far below the O2p VB, respectively. This is also the case for other monovalent cations, M = Cs, Na, and H, atomic orbitals of which take part in neither the VB nor the CB.

As-prepared four tantalates, $MCa_2Ta_3O_{10}$, were applied to photocatalytic decomposition of water under UV irradiation (Figure 4a). For unloaded samples, the rates of evolved H_2 as well as O_2 were low, depending upon M in the sequence of Na > Cs > H, but the ratio of H_2/O_2 evolved was close to the stoichiometry. For a $C_6H_{13}NH_3$-intercalated phase, much larger H_2 evolution (110 μmol·h^{-1}) occurred in an initial 8-h period,

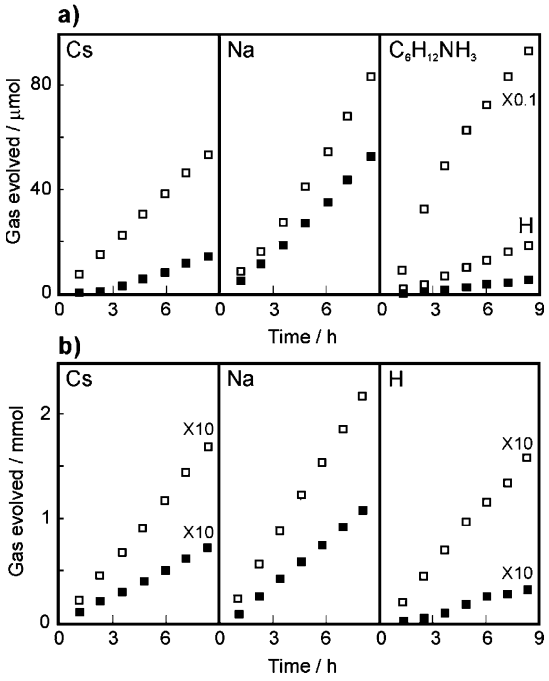

Figure 4. Gas evolution from water over (a) unloaded and (b) NiO_x-loaded $MCa_2Ta_3O_{10}$ (0.5 wt % Ni) under irradiation of UV light from a 400 W high-pressure Hg lamp. □ H_2, ■ O_2.

but after this, the evolution leveled off. The negligible evolution of O_2 implies that the $C_6H_{13}NH_3$ accommodated in the interlayer would be oxidized sacrificially. This was supported by the fact that the H_2 evolution was accompanied by the collapse of intercalated galley. The photocatalytic activity of these hydrated tantalates was also measured after loading partially oxidized nickel catalyst, NiO_x (0.5 wt % Ni), which is well-known as an active component for water splitting.[18,19] The oxidation state of Ni was confirmed to be 2+ by means of XPS. TEM observation suggested that NiO_x particles less than 10 nm in diameter were highly dispersed on the surface of planar crystallites of Cs, Na, and H phases (Figure S2, Supporting Information). As shown in Figure 4b, the effect of loading is obvious, but the rate of gas evolution was more strongly dependent on M, that is, the NiO_x-loaded Na phase exhibited the highest activity (>300 μmol-H_2·h^{-1}), whereas the NiO_x-loaded Cs and H phase was less active (<30 μmol-H_2·h^{-1}). The stoichiometric evolution of H_2 and O_2 from NiO_x supported on the Na phase increased monotonically with irradiation time, giving rise to the rates 308 and 158 μmol·h^{-1}, respectively. This corresponds to the apparent quantum yield of ca. 5%. The rate of photocatalytic gas evolution was measured for the Na phase as a function of Ni loading in Figure 5. The activity increased drastically with increasing the Ni loading up to 0.3 wt %, but further increase to 1.5 wt % led to almost the same activity. The cumulative amounts of H_2 and O_2 evolved over Ni-loaded samples during 8-h photoirradiation were more than the amount of tantalates, supporting that the reaction proceeded catalytically.

Reactivity of Hydrated Interlayer. As described above, the photocatalytic activity of hydrated Na phase for water splitting showed significant increase in the presence of Ni catalyst. This is in contrast to a low activity of the Ni-loaded H phase, which exhibits a hydrated structure as well as a band gap similar to those of the Na phase. No visible difference of NiO_x particle size, dispersion, and oxidation state was detected by TEM/XPS experiment. It is therefore suggested that the hydrous interlayer in these two phases is different from a viewpoint of reactivity. The hydration/dehydration behaviors of $MCa_2Ta_3O_{10}$ (M = Cs, Na, and H) were studied by measuring the X-ray basal reflection due to the layer structure (Figure 6). As-prepared $MCa_2Ta_3O_{10}$ (a) was first heated at 500 °C in vacuo for 5 h (b) and subsequently immersed in deionized distilled water with stirring at room temperature for 24 h (c). For M = Cs, negligible change of basal reflection at 2θ = ca. 6° is indicative of the totally anhydrous nature. By contrast, the basal reflection for the Na phase shifted to higher angles upon heating because of decreased interlayer spacing from 1.72 to 1.50 nm caused by elimination of water molecule from the interlayer (b). Because the anhydrous interlayer thus formed could be easily swelled by the subsequent immersion into water, reversible hydration/dehydration of the Na phase occurs very smoothly (c). Although the dehydration of interlayer was also observed for the H phase after heating (b), the rehydration could not be completed by subsequent immersion in water (c). This is indicative of the irreversible nature of a hydrated H phase.

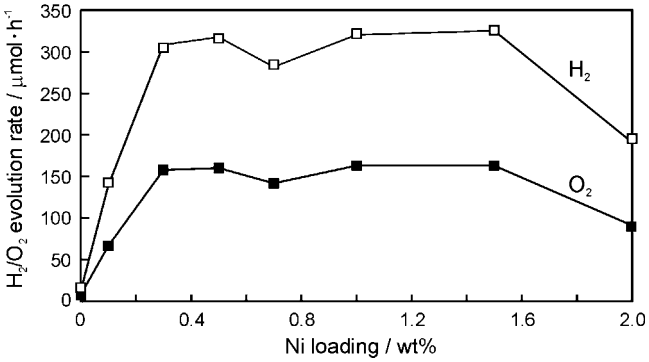

Figure 5. Effect of Ni loading on the rate of photocatalytic H_2 evolution from distilled water over $NaCa_2Ta_3O_{10}$. The reaction was carried out in an inner irradiation quartz cell under UV irradiation from a 400 W high-pressure Hg lamp.

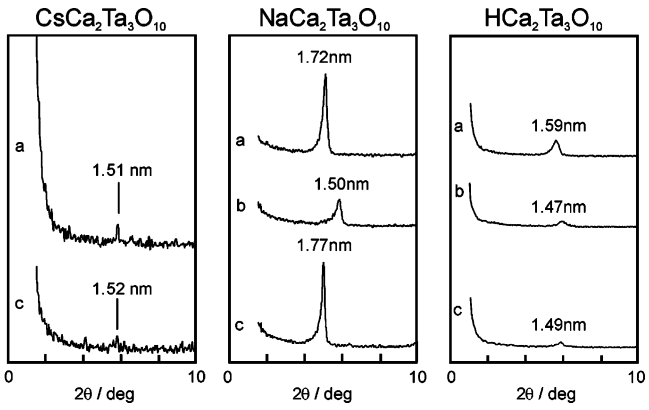

Figure 6. Change of XRD pattern of $MCa_2Ta_3O_{10}$ (M = Cs, Na, and H). (a) As-prepared, (b) heated at 500 °C in vacuo, and then (c) immersed in water at room temperature.

Isotopic Exchange of Interlayer Water. Hydration behavior of interlayer water was next studied by measuring infrared absorption spectra after treatment with D_2O (Figure 7). As-prepared Na phase with hydrated interlayer (a) exhibits broad bands due to OH stretching mode (ν_{OH}) at ca. 3450 cm^{-1} and two sharp bands due to HOH bending mode (δ_{HOH}) at 1700 and 1640 cm^{-1}. These bands disappeared after evacuation at 500 °C (c), but subsequent immersion into D_2O immediately yielded ν_{OD} (2500 cm^{-1}) and δ_{DOD} (1200 cm^{-1}), which is consistent with the accommodation of D_2O into the interlayer space (d). Peaks ascribable to ν_{OH}, δ_{HOH}, and δ_{HOD} (1400 cm^{-1}) are due to impurity H_2O originated from atmospheric water vapor. The result was in complete contrast to the fact that the immersion of H_2O-hydrated Na phase into D_2O showed

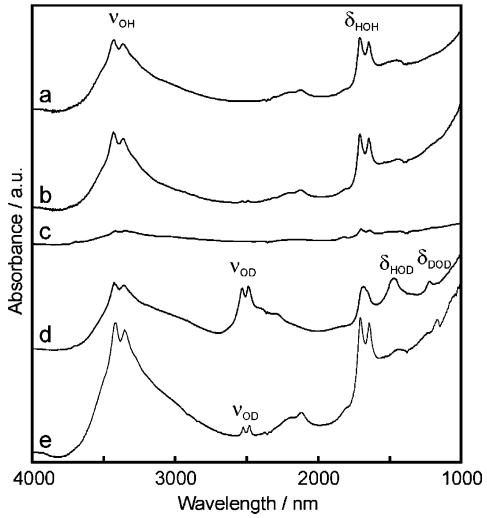

Figure 7. Change of FT-IR spectra of $NaCa_2Ta_3O_{10}$. (a) As-prepared H_2O-hydrated phase, (b) immersed in D_2O at room temperature, and (c) (a) heated at 500 °C in vacuo, and then (d) immersed in D_2O at room temperature, (e) as-prepared H_2O-hydrated phase immersed in D_2O under UV-irradiation.

negligible change in the spectra (b). This means that the exchange between interlayer H_2O and exterior D_2O is very slow. D_2O could be accommodated more rapidly when the as-prepared Na phase was immersed in D_2O under UV irradiation for 2 h (e). This may be explained by assuming that the interlayer active site can decompose H_2O to H_2/O_2 under UV irradiation and vacant sites thus formed accommodate D_2O from an exterior liquid phase.

To discriminate between photocatalytic reactions in the interlayer space and on the outer surface, we measured the isotopic ratios of gas evolved from $MCa_2Ta_3O_{10}$ (M = Cs and Na), which was dispersed in D_2O under UV irradiation from a 500 W Xe lamp (Figure 8). When the anhydrous Cs phase (0.5 wt % Ni loaded) was dispersed in D_2O, the gas evolved contained almost a constant amount of hydrogen ($HD/D_2 \leq 0.1$, $H_2/D_2 \leq 0.02$), which should be originated from impurity H_2O. Because of the difference in the dissociation energy, photocatalytic H_2O splitting proceeded ca. 3.5 times faster than that of D_2O. By contrast, the gas evolved in the first stage from H_2O-hydrous Na phase contained more hydrogen, and then, HD/D_2 and H_2/D_2 ratios decreased gradually to constant values, 0.28 and 0.03, respectively, which were ca. 2 times larger than those for the Cs phase.

These results represent that H_2O molecules between the layers of the Na phase take part in the photocatalytic gas evolution. With a progress of the consumption of H_2O in the interlayer close to the surface, D_2O molecules should be accommodated from an exterior liquid phase to interlayer to compensate the loss of water. In this way, the decrease of the isotopic ratios is in accord with decreased concentration of H_2O in the hydrated interlayer space. Because the interlayer photocatalytic reaction should take place in only a limited depth from the surface, where the UV light can reach, H_2O molecules would be therefore supplied from the bulk of tantalates. This is a possible reason the isotopic ratios became almost constant after several hours from the beginning of the reaction (Figure 8).

Role of Interlayer in Photocatalysis. The present study clearly demonstrated that the interlayer of the present layered tantalate plays a role of the active site for photocatalytic water splitting. An accelerated H_2 evolution from a $C_6H_{13}NH_3$-intercalated phase (Table 3) suggests that the organic moiety

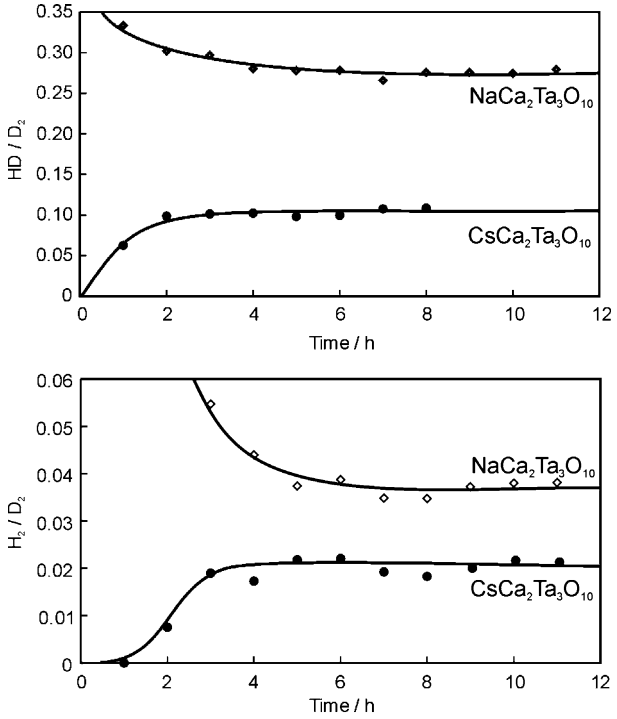

Figure 8. Isotopic distribution of photocatalytic gas evolution from D_2O over anhydrous Cs phase and H_2O-hydrated Na phase-loaded with 0.5 wt % Ni.

in the interlayer was reacted with holes as a sacrifice for H_2 evolution. Hydrogen evolution from H_2O-hydrated Na phase dispersed in D_2O also proves that H_2O molecule in the interlayer is decomposed to evolve H_2/O_2 even in the absence of sacrificial agents. This result is consistent with highest photocatalytic activity of hydrated Na phase for water splitting, which possesses the active site not only on the crystalline surface but also in the interlayer. On the contrary, this is not the case for the H phase, the hydration of which is not reversible as shown in Figure 6; that is, the low mobility of water molecules may not allow successive photooxidation reactions inside the interlayer. Therefore, the different effect of hydration may be associated with the mobility of water molecule inside the interlayer space. A negative effect of interlayer hydration may also be explained by deformation of H phase perovskite as evident from the XRD peaks (Figure 1), which exhibited broadening as compared to the parent Cs phase. Such deformation would yield structural defects, which would give rise to recombination centers of photogenerated carriers. Unlike the hydrated phase with M = Na and H, the Cs phase is very stable against hydration when suspended in water. The photocatalytic gas evolution over the Cs phase should therefore take place on the outer surface of the crystallites.

The present system is an n = three member of the Dion−Jacobson series layered structure, $A'[A_{n-1}Ta_nO_{3n+1}]$. The effect of hydration on the photocatalytic activity is different from that for double-layered tantalates ($n = 2$), $MLaTa_2O_7$ (M = Rb, Na, and H), in our previous work.[22,24] As in the present case, the Rb phase for $n = 2$ shows totally anhydrous nature, whereas the Na phase shows smooth and reversible hydration/dehydration. Nevertheless, the photocatalytic activity of hydrous $NaLaTa_2O_7$ for water splitting did not exceed that of anhydrous $RbLaTa_2O_7$ both in the absence and presence of NiO_x. As a possible reason for such a different feature between double- and triple-layered tantalates, we notice the dependence of electronic structure on the number of layers. As shown in Figure 3, four types of oxygen sites, O(1), O(2), O(3), and O(4), in the present

triple-layered perovskite ($n = 3$) contribute very differently to the total DOS. The O(1), O(2), and O(3) orbitals exhibit a considerable hybridization with Ta5d in the Ta−O network. By contrast, the terminating oxygen, O(4), which faces to the interlayer space, is less hybridized with Ta5d and contributes primary to the VB edge. Supposing the partial DOS of each oxygen reflects the spatial distribution of photogenerated holes in the hydrated phase, the O(4) site would contribute to the conversion of interlayer water to O_2. This is not the case for the double-layered perovskite ($n = 2$),[22,24] where the DOS peak due to terminating oxygen situates at ca. 1 eV below the VB edge. No remarkable interaction is expected between water molecules and holes in the interlayer of hydrated Na phase. These preliminary calculations may suggest that the number of perovskite layers, n in $A'[A_{n-1}Ta_nO_{3n+1}]$, is a key affecting the contribution of terminating oxygen to the total DOS profile, and thus the photocatalytic behavior of interlayer. To evidence this speculation, the electronic calculation is required to estimate the interaction between water molecules and perovskite slab in the hydrated interlayer, which would lead to a considerable modification of the VB structure. Further studies concerning the relationship between the band structure and the number of perovskite layers is now under investigation both from theoretical and experimental points of view.

Conclusion

In the present study, we have studied the electronic structure as well as crystal structure of Ruddledsen−Popper type triple-layered tantalate, $MCa_2Ta_3O_{10}$, with different interlayer cations (M = Cs, Na, H, and $C_6H_{13}NH_3$) to elucidate the role in the photocatalytic water splitting. The conclusions emerged from this study are as follows.

(1) The NiO_x-loaded tantalates exhibit different photocatalytic activity for overall water splitting under UV irradiation depending on the interlayer monovalent cations (M). The highest activity (H_2: >300 μmol·h^{-1}, O_2: >150 μmol·h^{-1}) was obtained for the hydrated Na phase in a wide range of loading 0.3−1.5 wt % Ni.

(2) The interlayer of hydrated phase act as active sites for photocatalytic reactions. The reversible hydration/dehydration behavior of the Na phase due to high mobility of water inside the interlayer space would be effective for the successive photocatalytic water splitting occurring therein.

(3) Judging from total and partial DOS for $CsCa_2Ta_3O_{10}$, four oxygen sites, O(1)−O(4), contribute quite differently depending on their position in the perovskite slab. The terminate oxygen O(4), which faces to the interlayer and contributes mostly to the valence band top, may lead to preferentially distributed holes on this site under photoirradiation.

Acknowledgment. The present study was financially supported by CREST and Grant-in aid for Scientific Research from the Ministry of Education, Science, Sports, and Culture.

Supporting Information Available: SEM photographs of $MCa_2Ta_3O_{10}$ (M = Cs, Na, and H) and TEM photograph of $CsCa_2Ta_3O_{10}$ loaded with 0.5 wt % Ni. This material is available free of charge via the Internet at http://pubs.acs.org.

References and Notes

(1) Schaak, R. E.; Mallouk, T. E. *Chem. Mater.* **2002**, *14*, 1455.
(2) Dion, M.; Ganne, M.; Tournoux, N. *Mater. Res. Bull.* **1981**, *16*, 1429.
(3) Dion, M.; Ganne, M.; Tournoux, N.; Revez, J. *Chim. Miner.* **1984**, *21*, 92.
(4) Ruddlesden, S. N.; Popper, P. *Acta Crystallogr.* **1957**, *10*, 538.
(5) Gopalakrishnan, J.; Bhat, V. *Inorg. Chem.* **1987**, *26*, 4301.
(6) Domen, K.; Naito, S.; Ohnishi, T.; Tamaru, K. *Chem. Phys. Lett.* **1982**, *92*, 433.
(7) Inoue, Y.; Kubokawa, T.; Sato, K. *J. Chem. Soc., Chem. Commun.* **1990**, 1298.
(8) Inoue, Y.; Niiyama, T.; Asai, Y.; Sato, Y. *J. Chem. Soc., Chem. Commun.* **1992**, 579.
(9) Uchida, S.; Yamamoto, Y.; Fujishiro, Y.; Watanabe, A.; Ito, O.; Sato, T. *J. Chem. Soc., Dalton Trans.* **1997**, *93*, 3229.
(10) Kudo, A.; Tanaka, A.; Domen, K.; Maruya, K.; Aika, K.; Ohnishi, T. *J. Catal.* **1988**, *111*, 67.
(11) Takata, T.; Shinohara, K.; Tanaka, A.; Hara, M.; Kondo, J. N.; Domen, K. *J. Photochem. Photobiol.* **1997**, *106*, 45.
(12) Kudo, A.; Kato, H. *Chem. Lett.* **1997**, 867.
(13) Ihihara, T.; Nishiguchi, H.; Fukamachi, K.; Takita, T. *J. Phys. Chem.* **1999**, *103*, 1−3.
(14) Machida, M.; Yabunaka, J.; Kijima, T. *Chem. Commun.* **1999**, 1939.
(15) Machida, M.; Yabunaka, J.; Kijima, T. *Chem. Mater.* **2000**, *12*, 812.
(16) Toda, K.; Teranishi, T.; Ye, Z.-G.; Sato, M.; Hinatsu, Y. *Mater. Res. Bull.* **1999**, *34*, 971.
(17) Toda, K.; Sato, M. *J. Mater. Chem.* **1996**, *6*, 1067.
(18) Domen, K.; Naito, S.; Soma, M.; Ohnishi, T.; Tamaru, K. *J. Chem. Soc., Chem. Commun.* **1980**, 543.
(19) Domen, K.; Kudo, A.; Ohnishi, T. *J. Catal.* **1986**, *102*, 92.
(20) Jones, R. O.; Gunnarsson, O. *Rev. Mod. Phys.* **1989**, *61*, 689.
(21) Blaha, P.; Schwarz, K.; Luitz, J. *WIEN97*; Vienna University of Technology, Vienna, 1997. [Improved and updated UNIX version of the original copyrighted WIEN code, which was published Blaha, P.; Schwarz, K.; Sorantin, P.; Tricky, S. B. *Comput. Phys. Commun.* **1990**, *59*, 399.]
(22) Machida, M.; Yabunaka, J.; Kijima, T.; Matsushima, S.; Arai, M. *Int. J. Inorg. Mater.* **2001**, *3*, 545.
(23) Machida, M.; Murakami, S.; Kijima, T.; Matsushima, S.; Arai, M. *J. Phys. Chem. B* **2001**, *105*, 3289.
(24) Machida, M.; Miyazaki, K.; Kijima, T.; Matsushima, S.; Arai, M. *J. Mater. Chem.* **2003**, *13*, 1433.